Biolasing from Individual Cells in a Low-Q Resonator Enables Spectral Fingerprinting

Advanced Optical Materials

Biolasing from individual cells in a low-Q resonator enables spectral fingerprinting

--Manuscript Draft--

Manuscript Number:	adom.201901573R1
Full Title:	Biolasing from individual cells in a low-Q resonator enables spectral fingerprinting
Article Type:	Full Paper
Section/Category:	
Keywords:	biolasing; cell distinction; PCA; scattering; biosensing
Corresponding Author:	Damiano Genovese Universita di Bologna Bologna, ITALY
Corresponding Author Secondary Information:	
Corresponding Author's Institution:	Universita di Bologna
Corresponding Author's Secondary Institution:	
First Author:	Damiano Genovese
First Author Secondary Information:	
Order of Authors:	Damiano Genovese
	Dedy Septiadi
	Valentin Barna
	Dhruv Saxena
	Riccardo Sapienza
	Luisa De Cola
Order of Authors Secondary Information:	
Abstract:	Lasing from cells has recently been subject of thorough investigation because of the potential for biosensing. Yet, lasing from individual cells has only been observed in presence of high-quality resonators, resulting in limited dependence of the lasing properties on the cellular microenvironment. Here lasing is triggered by cells floating in a low quality factor resonator composed of a disposable PMMA cell counting-slide, hence in absence of conventional high-reflectivity optical cavities. The exceptional spectral narrowing and the steep slope increase in the input-output energy diagram prove the occurrence of laser action in presence of cells. Biolasing obtained in these conditions is an intrinsically dynamic signal, with large fluctuations in intensity and spectrum determined by the optical properties of the individual cell passing through the pump beam. Numerical simulations of the scattering efficiency rule out the possibility of optical feedback from either WGM or multiple scattering within the cell, and point to a strong enhancement of directional scattering field as the crucial contribution of cells to the laser action. Finally, principal component analysis of lasing spectra measured from freely diffusing cells yields spectral fingerprints of cell populations, which allow discriminating cancer from healthy Rattus glial cells with a high degree of confidence.
Additional Information:	
Question	**Response**
Please submit a plain text version of your cover letter here.	Dear Editor, Please find enclosed the manuscript entitled: Biolasing from individual cells in a low-Q resonator enables spectral fingerprinting, which we are submitting to the Advanced Optical Materials as a Full Paper.

	We believe that this manuscript matches well with the interdisciplinary purpose of the Journal, as: -it demonstrates an unconventional light-cell interaction with interdisciplinary application potential: biological cells here provide a substantial contribution to triggering laser action, even in a low Quality factor PMMA cell-counting slide, hence without the need for conventional high-reflectivity resonators; -it opens to a ready method in cancer research for fast, high-throughput analysis; -both experimental and simulation approaches are thoroughly carried out and discussed, demonstrating the scientific validity and solidity of the experimental results; -the simplicity of the method used to achieve directional, intense and highly efficient laser emission makes it easily applicable to a variety of scientific purposes. We have highlighted the results in a form that can reach a broad scientific community. The physical meaning as well as the biological impact of the unconventional light-cell interaction are demonstrated and discussed. For these reasons, we believe that this work can be a stimulating contribution for a wide, interdisciplinary community, and therefore it deserves the honour to be considered for publication in Advanced Optical Materials. We also state here that: • All authors agree with the submission; • The work has not been published or submitted for publication elsewhere, either completely or in part, or in another form or language; • No materials are reproduced from another source; • We declare that we do not have any conflict of interest. Looking forward to your decision, Best regards Damiano Genovesea and Luisa De Colab a] Dipartimento di Chimica “Giacomo Ciamician”, Università di Bologna, via Selmi 2, Bologna, 40126, Italy b] Institut de Science et d'Ingénierie Supramoléculaires, Université de Strasbourg, 8 allée Gaspard Monge, 67083 Strasbourg, France Email: damiano.genovese2@unibo.it, decola@unistra.fr
Do you or any of your co-authors have a conflict of interest to declare?	No. The authors declare no conflict of interest.

WILEY-VCH

Biolasing from individual cells in a low-Q resonator enables spectral fingerprinting

Dedy Septiadi, Valentin Barna, Dhruv Saxena, Riccardo Sapienza, Damiano Genovese and Luisa De Cola**

Dr. D. Septiadi, Prof. L. De Cola, Institut de Science et d'Ingénierie Supramoléculaires, Université de Strasbourg, 8 allée Gaspard Monge, Strasbourg, 67083, France
Prof. V. Barna, Dr. D. Genovese, Institute of Nanotechnology, Karlsruhe Institute of Technology, KIT Campus North, Hermann-von-Helmholtz-Platz 1, Eggenstein-Leopoldshafen, 76344, Germany
Prof. V. Barna, University of Bucharest, Faculty of Physics, PO Box Mg-11, 077125, Bucharest, Romania
Dr. D. Saxena, Prof. R. Sapienza, The Blackett Laboratory, Department of Physics, Imperial College London, London, SW7 2AZ, UK
Dr. D. Genovese, Dipartimento di Chimica "Giacomo Ciamician", Università di Bologna, via Selmi 2, Bologna, 40126, Italy
E-mail: damiano.genovese2@unibo.it, decola@unistra.fr

Keywords: biolasing, cell distinction, PCA, scattering, biosensing

Lasing from cells has recently been subject of thorough investigation because of the potential for sensitive and fast biosensing. Yet, lasing from individual cells has only been observed in presence of high-quality resonators, resulting in limited dependence of the lasing properties on the cellular microenvironment. Here lasing is triggered by cells floating in a low quality factor resonator composed of a disposable PMMA cell counting-slide, hence in absence of conventional high-reflectivity optical cavities. The exceptional spectral narrowing and the steep slope increase in the input-output energy diagram prove the occurrence of laser action in

presence of cells. Biolasing obtained in these conditions is an intrinsically dynamic signal, with large fluctuations in intensity and spectrum determined by the optical properties of the individual cell passing through the pump beam. Numerical simulations of the scattering efficiency rule out the possibility of optical feedback from either WGM or multiple scattering within the cell, and point to a strong enhancement of directional scattering field as the crucial contribution of cells to the laser action. Finally, principal component analysis of lasing spectra measured from freely diffusing cells yields spectral fingerprints of cell populations, which allow discriminating cancer from healthy Rattus glial cells with a high degree of confidence.

1. Introduction

Fluorescent dyes are a common bioimaging tool, whose spontaneous emission is used to monitor in real time and real space the activity of cells, organelles and biomolecules[1] with high resolution and sensitivity.[2] Nonetheless, in the presence of strong excitation fields and of optical feedback, stimulated emission can overcome fluorescence and eventually lead to laser action. Lasing, compared to spontaneous emission, carries information not only on the solvating environment in the direct vicinity of the dyes, but also on the optical system (e.g. cavities, microresonators or scatterer density) that generates the amplification, since it determines at a large extent the allowed spectral and spatial properties of laser emission, i.e., the lasing modes. Recently, different biological materials have been shown to support light

amplification from suitable chromophores:[3] laser action has been observed from biomaterials in the different forms of rigid/hard scaffolds (such as protein crystals,[4] disordered protein scaffolds,[5] butterfly wings,[6]-[7] skeleton,[8] etc.), soft materials,[9] tissues[10,11] and interestingly even from individual cells,[12–15] based on various amplification schemes. Cellular lasing, i.e. lasing from individual cells, has been proposed as a promising novel concept with potential for enhanced sensing.[16,17]

So far it has been ~~only~~ achieved as a result of the amplification provided by laser cavities[12] or microresonators[13–15] while lasing from an isolated individual cell has proven to be elusive, and only observed in isolated adipocytes featuring very large oil droplets (~45 μm). For cells inside a cavity composed of two reflective mirrors, the refractive index contrast between a cell and its surrounding medium has been found to lower the threshold for lasing, due to the so-called "lens-effect".[18,19] In these conditions, the laser threshold has been reported to carry information on cellular properties (such as the hydration level)[18] and it has been used to discriminate cancer from healthy cells.[20]

In this contribution, we describe a new experimental approach in which light amplification is generated from an individual cell driven by cell morphology and optical contrast. Based on this approach a new role may emerge for the cells, which not only act as a container of active medium (i.e. the laser dyes) but also play a fundamental role in the amplification process. We therefore investigate numerically the role of the refractive index contrast within a cell and

between the cell and the surrounding medium, in order to ascertain the origin of light amplification. Finally, we analyse the relationship between cell and amplified emission properties, highlighting the key parameters of light amplification that can be exploited to discriminate two different groups of cells, and in particular healthy from cancerous Rattus glial cells.

2. Results

2.1. Cell sample design and preparation

We investigate the optical properties of cancerous (C6 glioma) and healthy (Astrocyte) Rattus glial cells. Cell trypsination followed by paraformaldehyde fixation are performed before incubating cells in Rhodamine 6G (R6G) staining solution (0.9 mM in DMSO for 30 minutes), to obtain highly dye-doped, fixed cells detached from the surface and showing a roughly spherical shape (10-20 µm in diameter). Fluorescence confocal microscopy analysis of cell samples deposited on microscope slides reveals that fluorescent intensity of intracellular dyes are 2 to 4 folds brighter than the supernatant (**Figure 1a-1c, S1** in the Supplementary Information). The cell samples are then transferred in cell counting slides without further washing (**Figure 1e**), which are held vertical in order to minimize cell adhesion on the plastic walls. The observation system is finally composed of a 100 µm thick

chamber delimited by two facing Poly(methyl methacrylate) (PMMA) walls (thickness 700 µm each), resulting in very weak reflection at the system interfaces (transmittance, *T*~96% at each wall).

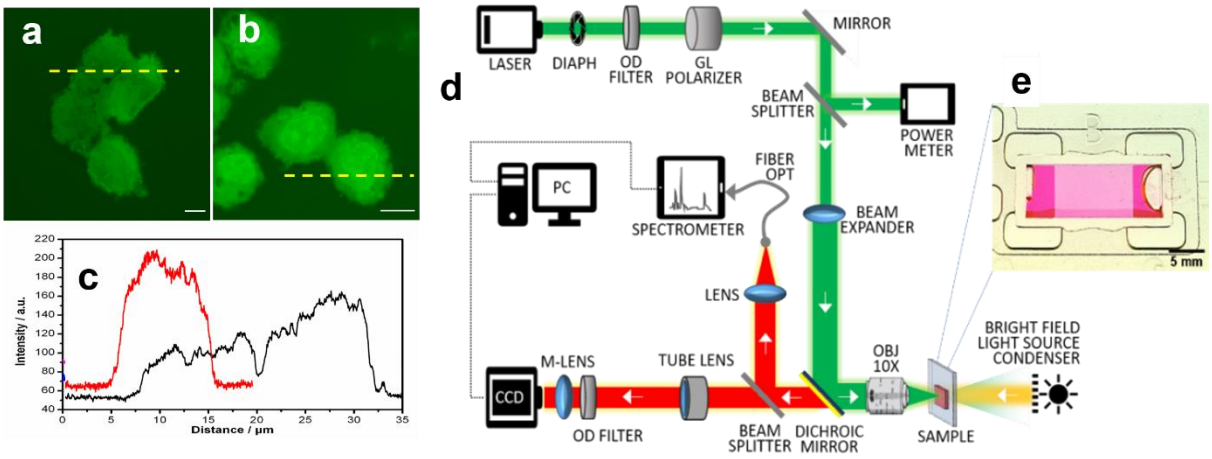

Figure 1. Fluorescence confocal micrographs of the cell samples Astrocyte and C6 Glioma (**a** and **b** respectively, scale bar 5 µm) and their intensity profiles across yellow dashed lines (**c**, black and red lines respectively). Samples were excited using λ_{exc} 514 nm and fluorescence signal was collected from 520 nm to 723 nm. **d**. Schematic representation of the optical set-up used in the experiment. The optical line consists of a pulsed Nd:YAG laser (frequency of 10Hz, pulse duration 8 ns) coupled to a MOPA (Master Oscillator Power Amplifier), a diaphragm, optical density filters, a Glann-Laser polarizer, a mirror, a beam splitter that reflects a known fraction of the beam into a power meter, a beam expander, dichroic mirror, a 10x objective and a bright field illuminator on the opposite side of the sample, a beam splitter that separates the detection into the imaging arm (a CCD camera with tube lens and magnification lens) and the spectroscopy arm (an optical fiber with focusing lens connected to multichannel spectrometer for spectral analysis). **e**. A photograph of a cell sample in cell counting slide under ambient light. The picture is taken 24h after the experiment and shows the cells sedimented at the bottom.

The samples are excited at room temperature with a pulsed laser system (λ_{exc}=540 nm, frequency 10 Hz, pulse duration 8 ns) in a fluorescence microscopy setup, with the excitation beam reflected by a dichroic mirror and focused onto the sample with a 10× objective lens (numerical aperture, NA = 0.25) (**Figure 1d**), yielding a beam waist of approximately 20 μm in the focal point, and an estimated Rayleigh length of 250 μm. The emission is collected by the same objective and transmitted through the dichroic mirror to a beam splitter. A CCD camera is used to image the sample and a high-resolution spectrometer provides single shot emission spectra.

1.2 Spectral and image analysis

By synchronizing spectral acquisition with CCD imaging at the same frequency of the pump laser (10 Hz), spatial distribution of the emission signal corresponding to each individual pump shot is obtained, while the spectrometer monitors the spectral features of the imaged emission. By adjusting the power of the excitation laser at 1.5 μJ/pulse (120 mJ/cm^2), we record markedly different emission bursts when a cell is in the excitation focus, compared to the case in which no cell (thus only dye-doped supernatant) is present across the pump beam (**Movie M1**). In particular in the latter case a constant background is recorded both by the CCD (**Figure 2a,d**) and by the spectrometer, which in these conditions records only bright field light and fluorescence (**Figure 2f,g**). On the contrary, when a cell transits across the

excitation beam, strong emission bursts transitorily appear on the CCD, localized in correspondence of the cell, while the corresponding spectrum is characterized by the presence of multiple, very narrow spikes randomly distributed in a ca. 5 nm wavelength range and of width 0.4 nm (see **Figure 2h-n**).

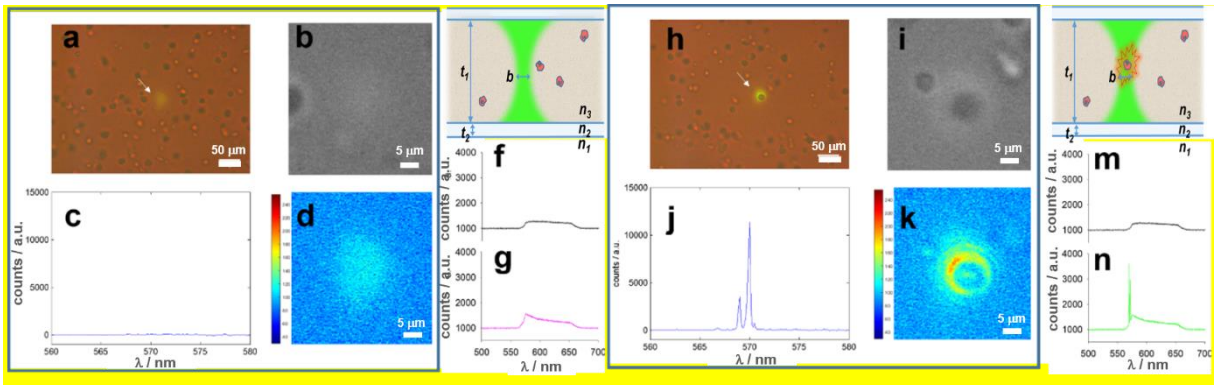

Figure 2. Extracts from **Video M1** showing fluorescence from supernatant (**a-d**, no cells in the excitation beam) and light amplification (laser action) from a cell passing through the excitation beam (**h-k**), under constant excitation conditions (1.5 µJ/pulse). Each video frame in movie M1 shows synchronized colour image of the sample on a RGB CCD camera (**a**, **h**), emission spectra subtracted of the constant background taken with an Ocean Optics HR4000 Spectrometer (**c**, **j**, while the constant background is shown in **g**), the red channel of the CCD image in grayscale, which contains minimal emission information and can thus be used as bright field image (**b**, **i**) and green channel of the CCD image in "jet" color scale (**d**, **k**) that contains emission information and can be taken as fluorescence images. Sketches of the cross section of the experimental system (not to scale) in absence (**e**) and in presence of cells (**l**) passing through the excitation beam. t_1= thickness of the chamber, 100 µm. t_2= thickness of the PMMA walls, 700 µm. n_1, n_2 and n_3 are the relevant refractive indices, respectively of air (1.00), PMMA (1.49), and the supernatant (DMSO, 1.48). Spectra of the background due to the only bright field illumination (**f**, **m**) are compared with spectra recorded with both bright field illumination and laser excitation in absence of cells (**g**) and in presence of cells passing through the laser beam (**n**); note that all recorded spectra are cut in the observation window (570-660 nm) by the dichroic and emission filters.

In these experimental conditions, emission bursts from an individual cell can be continuously recorded over hundreds of shots, and if no cells are transiting in the vicinity of the pump beam, only a constant fluorescence background is observed both on the CCD and on the spectrometer (**Movie M1**).

Selected CCD images of cell-triggered light amplification show that the emission distribution generally follows the shape of the cell passing through the beam and of its internal compartments (**Figure 3e-i**). This suggests that the weakly scattering biological material contained in the cells, and particularly in the membranes and in the organelles,[21,22] plays a key role in triggering the light amplification process.

Increasing the pump power, in the presence of cells, we observe a transition from a regime of pure fluorescence (at low pump power, whose intensity increases linearly with the excitation power) to a regime at which the sudden emission bursts described above are observed. This transition occurs across a 300 nJ range, at approximately 500-1000 nJ/pulse (40-80 mJ/cm^2) for the different cell samples (**Figure 3a-b**). The light emission integrated in the range 565-575 nm (where light amplification peaks arise) versus the input laser power (**Figure 3a**), displays the expected laser behavior: the slope deviates from the initial value in concomitance with the observation of the first emission spikes (when pump power reaches 800 nJ/pulse, i.e. 65 mJ/cm^2 **, Figure S2** in the Supplementary Information), but with large fluctuations of the recorded spectra (witnessed by the huge error bars in the range 1.2-1.6 μJ).

These fluctuations, due to cell diffusion and cell-to-cell variations, make it difficult to properly assess the lasing threshold. The error bars appear to decrease much above threshold (1.8 μJ), when the presence of multiple spikes in the emission spectra results in smaller intensity fluctuations. For pump powers larger than 2 μJ/pulse (160 mJ/cm^2) the cells suffer relatively fast damage and therefore we limit our analysis to powers below 2 μJ/pulse to prevent biased observations. Indeed, at pump energies close to the lasing threshold individual cells can be continuously observed for minutes (thousands of pulses), while at pump power larger than 2 μJ/pulse cells and dyes typically degrade, and the signal is lost within few seconds (tens of emission bursts).

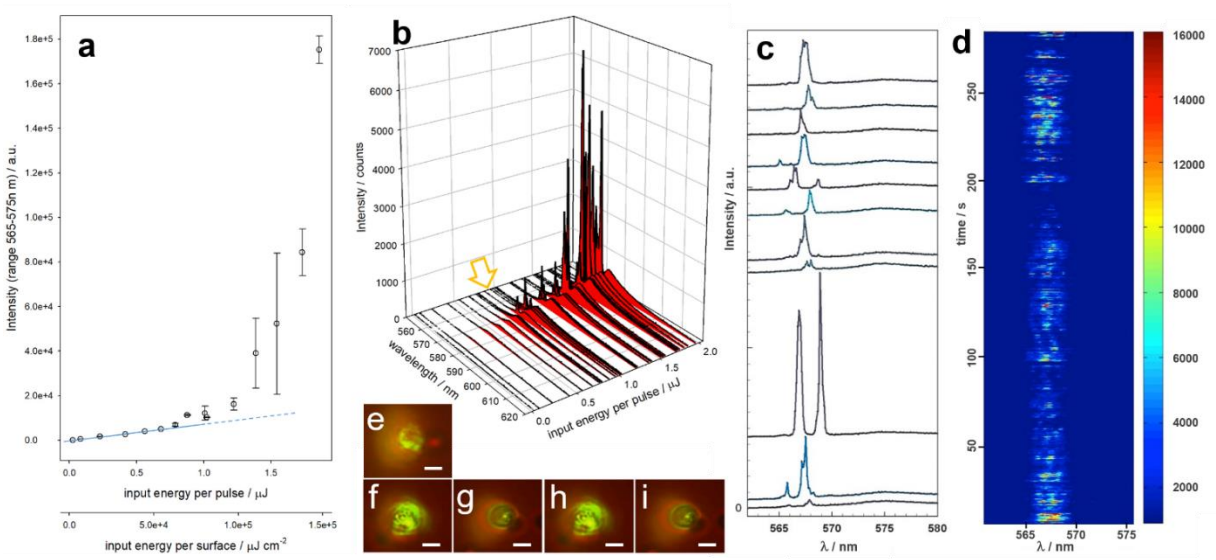

Figure 3. **a**. Input versus output diagram showing the transition from fluorescence to light amplification of C6 glioma cells; emission intensity is integrated in the range 565-575 nm; the blue dashed line highlights the linear increase of fluorescence emission; error bars are

calculated from 10 spectra from different cells. **b**. Emission spectra of cells transiting across the excitation beam, at increasing input energy; the yellow arrow indicates the onset of light amplification. **c**. Selected amplified emission spectra from C6 glioma cells taken at constant excitation power, P_{exc} = 1.5 μJ/pulse. The broad band centered at 575 nm is fluorescence. **d**. Time sequence of single shot emission spectra taken in a standard experiment. **e-i**. Selected CCD images of individual C6 glioma cells transiting through the excitation beam, scale bar 5 μm.

Figure 3c-d shows that the spectra of amplified emission feature peaks, which are "randomly" distributed in wavelength and in time. Both the spectra originated from different cells and from the same cell excited with subsequent pulses show emission spikes at wavelengths that change pulse-to-pulse, and with varying spacing between spikes, as shown in the spectral time series in **Figure 3d**. This suggests that the mechanism responsible for light amplification is randomly determined by the specific physico-chemical parameters of the cell passing in the beam focus and of its subcomponents.

1.3 Simulation of light scattering induced by cells

We attribute the shot-to-shot variation in the lasing spectrum to the variability of the cell optical response. The cell optical properties are sketched in **Figure 4a**, for an idealized spherical cell (12 μm in diameter) with a nucleus with high refractive index (n_{core} = 1.5), surrounded by cytoplasm with lower refractive index (n_{cell} = 1.33-1.47), immersed in either water (n_{H2O} = 1.33) or DMSO (n_{DMSO} = 1.48), using values common in the literature.[23,24]

Given the large size of the cell compared to the light wavelength and the low refractive index contrast, the exact shape of the cell does not significantly affect the results. Numerical simulations of light scattering were made by finite-difference time-domain (FDTD) solution of the Maxwell's equations using Lumerical.[25] The profiles of electric field intensity in **Figure 4c-e** show large forward scattering and focusing of the incident light (yielding the lensing effect), with an increase in the pump intensity by up to a factor of 50 in a volume of around $(\lambda/2n)^3 \approx 0.2\ \mu m^3$. This local field enhancement increases the probability of stimulated emission and is the principal mechanism for the observed strong light amplification in the presence of cells in our experiments. The high density of laser dye within the cells also facilitates gain.

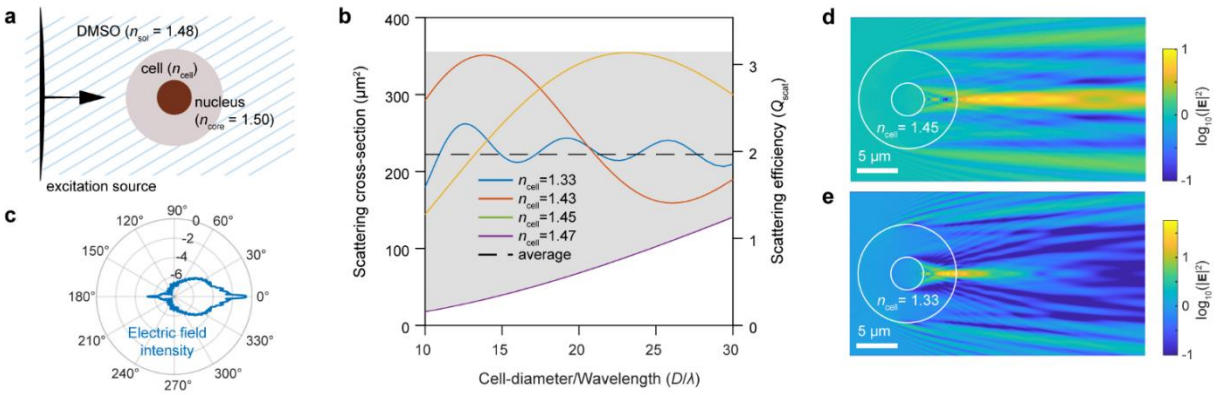

Figure 4. **a**. Schematic illustration of a cell in DMSO, modelled as a sphere with a core-shell structure. The nucleus is one third the size of the cell (D = 12 μm, nucleus = 4 μm). **b**. Scattering cross-section and scattering efficiency (cross-section/geometrical area) of the cell calculated by 3D Finite-Difference Time-Domain (FDTD) simulations. The cross-section is shown as a function of D/λ for different cell refractive indices (colored solid lines). On average, the cross-section is 220 μm^2 (dashed line). The grey region indicates the range of possible values due to

variation in cell index/shape. **c** Far-field intensity distribution of the scattered fields shown in log scale on a polar plot. **d-e**. Electric field intensity profile in the cross-section of a cell (λ = 570 nm) with cell index 1.45 and 1.33, respectively. The plane wave is incident from the left hand-side in both images.

The lasing spectra with sharp peaks however suggests existence of a closed cavity and cannot be accounted for by gain narrowing in an open cavity alone. Cavity resonances supported by the cell however can be ruled out, owing to the very low Q factor of the optical modes supported by biological cells (~1), in particular when DMSO is the main component of the supernatant. Multiple scattering[26,27] within the cell is also unlikely, due to the low index variation within the cell, or within the cell solution, which results only in large forward scattering (as shown by FDTD simulations for all refractive indices n_{cell} = 1.33-1.47, **Figure 4b**) as possible explanations for the observed lasing behaviour.

The only other feedback mechanism in our sample is reflection from the large polymeric cell, made of the two 700-µm-thick PMMA layers separated by a 100 µm gap, containing the supernatant with cells (i.e. total cavity length of 1.5 mm). Although the PMMA/air interface provides minimal reflectance (of ~4%), the long cavity length results in an appreciable Q factor of a few thousands. We argue that this is the principle mechanism for the observed narrow features in the lasing spectrum. The biological cells here provide a crucial role to facilitate lasing, which would otherwise be difficult to attain due to misalignment of the cavity mirrors. As shown in **Figure 4d-e**, the cells act as a micro-lens, and so can stabilize the laser

resonator by redirecting the diffracted rays towards the optical axis.[18] To test the effectiveness of the cells in stabilizing the laser resonator, the experiment was repeated with the cells and supernatant sandwiched between two glass slides with one of the slides tilted at an angle. Lasing was still observed from the cells for tilt angles of 1 degree (see **Figure S3** in the Supplementary Information), but not at large angles (5 degrees). This result is consistent considering the cell dimensions and focal length. A small tilt of 1 degree for example, results in a path difference of 3.5 μm, and so the reflected light still pass through the cell, whereas with a 5 degree tilt the offset is 17.5 μm, which is larger than the cell diameter and after one round trip the rays are already outside the pumped region.

1.4 *Cell distinction via PCA of amplified emission spectra*

Light amplification is triggered by the cells due to their refractive index contrast and high dye concentration. Refractive index distribution, in particular, is relevant in this investigation because it is tightly related to cell morphology, lifecycle and phenotype.[28,29] Therefore, we have investigated the possibility of extracting characteristic information on cells from their amplified emission spectra.

In order to demonstrate the relation between cell structure and emission features, useful to differentiate cancer from normal cells, we developed a method based on spectral analysis. The strategy employs time series of spectra, which we analyse with principal component analysis

(PCA) in order to distinguish cells from similar tissues but with different status, either healthy or cancerous. In particular, we processed time series of at least 10,000 spectra acquired in continuous (containing at least 1000 amplified emission spectra) from the two samples of cells, i.e. C6 glioma and Astrocyte.

The random nature of amplified emission spectra also causes large intensity fluctuations, even between consecutive shots. Spectra are grouped in sets based on peak intensity, and then analysed to retrieve similarities within the same set and among different cells of the same stock. In particular, given two datasets, respectively for cancerous and healthy cells, average spectra are calculated for each dataset and used to extract principal component (PC) loadings. Loadings are in turn used to calculate PC scores for each single-shot spectrum. The resulting scores of the first two PCs (i.e. the ones with highest variances) are plotted for visual comparison of the separation between the two different cell samples and of the spectral spread of each sample (**Figure 5**).

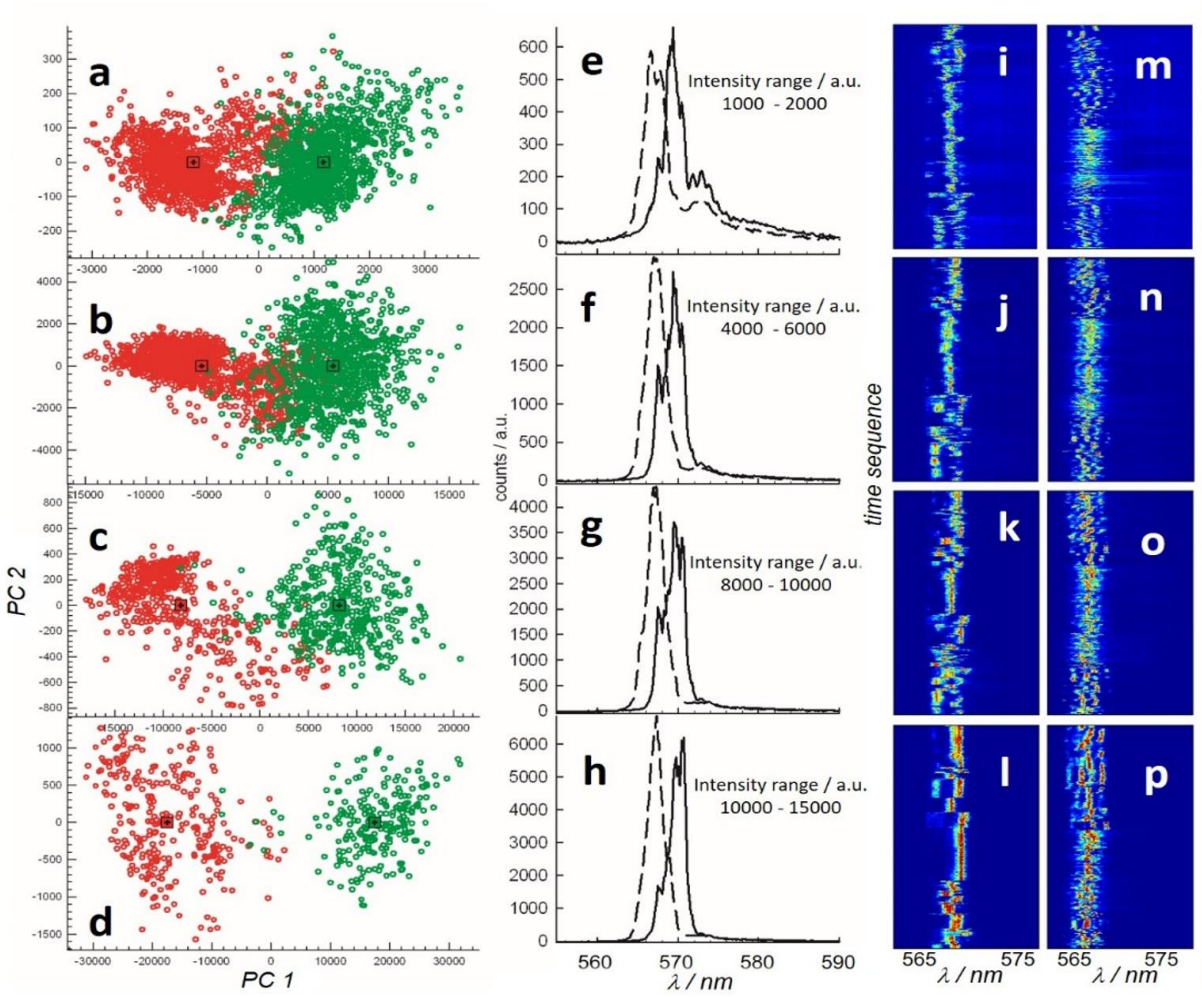

Figure 5. The four rows from top to bottom display data relative to spectra with peak intensity in ranges 1,000-2,000 counts, 4,000-6,000 counts, 8,000-10,000 counts and 10,000-15,000 counts, respectively, as also indicated in plots of average spectra (**e-h**). **a-d**. PC scores of single shot spectra of C6 glioma cells (red) and Astrocytes (green) with increasing peak intensities. The crossed squares indicate the scores of the average spectra. The scores are calculated from loadings obtained from the average spectra, which are shown in diagrams **e-h** (C6 glioma solid lines, Astrocytes dashed lines). Maps **i-l** show the time series of C6 glioma amplified emission spectra in selected intensity ranges, while maps **m-p** show the time series of selected Astrocyte amplified emission spectra.

Looking only at the average spectra used to extract PC loadings, it is evident how the spectral difference, and thus the possibility to discriminate cells, is very modest (**Figure 5e-h**). On the contrary, PC scores relative to single shot spectra taken from cancer versus healthy Rattus glial cells (respectively C6 glioma and Astrocyte) reveal that the two sets of spectra lie in two clearly distinct regions of the diagram (**Figure 5a-d**). Moreover, the separation between the two populations of PC scores largely increases and the overlap vanishes when the most intense amplified emission spectra are considered. The here described method yields thus new parameters, i.e. the PC scores, that are easier to handle compared to the spectra, and that can be conveniently employed to put in evidence subtle spectral differences. We demonstrate that this analysis allows for distinction of cancer from healthy Rattus glial cells (C6 glioma –cancerous– vs Astrocyte –healthy–) with a very good level of confidence.
In addition, it has to be noted that the variance of the first PC is as high as 99% in the highest intensity range for Rattus glial cells, thus allowing cell distinction based on only one parameter and a consequently easier representation through 1D graphs, such as the histograms of PC1 scores (**Figure S4** in the Supplementary Information).

2. Discussion

The experimental evidence of the concomitance of light amplification with the presence of cells in the excitation beam strongly suggests that the intrinsic physico-chemical properties of

cells play a predominant and active role in this phenomenon. Concerning the reasons why cells support light amplification and eventually laser action, we take into consideration gain enhancement (due to dye concentration and brightness) and amplification mechanisms (due to refractive index contrasts). On the one hand, the gain across the excitation beam increases due to the higher dye concentration in the cells compared to the supernatant (up to 2-4 times locally, **Figure 1a-d**), but such increase only accounts for a 10-20% gain enhancement across the whole excitation path (about 100 μm). On the other hand, it is well known that cell compartmentalization produces significant refractive index contrast within a cell, among the different compartments, and with the external environment.[23,28–30] The refractive index in cells, already acknowledged as a key parameter for both basic understanding of cell function and interpretation of pathological state, is directly related to intracellular local mass and concentration, thus yielding fundamental biophysical information about composition and organizational structure of cells. Variations in cellular refractive index can result in altered tissue light scattering effects, often related to tissue pathology,[31] and in various diseases such as in hematologic contexts.[32] However, efforts to experimentally address the refractive properties of cells have long been impeded by experimental difficulties. ~~, and only recently have some successful approaches been presented that, though, often concern the average refractive index of a cell population suspended in a medium, with no information on the refractive index distribution.~~ The here reported light amplification phenomenon directly stems

from cellular refractive index, and from refractive index contrast within the cell; as such, it carries an important potential to indirectly address –by means of a fast and information-rich technique– the single-cell analysis of refractive index-related properties of cells. Such fast spectral analysis of cellular lasing may be implemented in cytometry techniques, adding an instrument to investigate cellular properties related to refractive index distribution even below the diffraction limit.

It has to be highlighted that in this study, differently than in recent reports on cellular lasing, cells are not placed within a high reflectivity laser cavity,[10,12] nor do they contain microresonators.[11,13] Reflectance at the walls is indeed very poor and external agents such as microbeads or scattering nanoparticles/nanocrystals are not introduced in the system. Humar and Yun reported that cell lasers consisting of dye-doped cells embedded between two high reflective distributed Bragg reflector (DBR) mirrors, in an all-similar experimental setup with ns pulsed pump laser, display a laser threshold of ca. 45 nJ / pulse.[18] In such a case DBR mirrors provided the light confinement required for amplification, and the cells play only a minor role in reducing the laser thresholds owing to a thoroughly described "lens effect".[18,19] In our experiments we observe laser emission with threshold only 10-20 times higher than this previously reported threshold in a DBR. In the here discussed case cells provide an essential contribution in triggering laser action. Our simulations of light scattering demonstrate that amplification of spontaneous emission can be greatly facilitated in presence of cells owing to

the strongly enhanced directional light scattering and to light focusing, in addition to gain enhancement due to the higher concentration of dye inside cells. The difference in refractive index within the cell, between the various compartments, is thus responsible for directional scattering and focusing of light that, under specific conditions of high gain, can give rise to phenomena of light amplification and eventually laser emission.

In summary, lasing in our experiments is facilitated by the external cavity within which the dye and biological cells are placed. However, due to the low Q factor of this external cavity, the cells provide important functions of reducing the lasing threshold and stabilizing the laser cavity. As a result, we observed spectral signatures that allowed to distinguish with high degree of confidence C6 glioma –cancerous– from Astrocyte –healthy– Rattus glial cells. ~~Because of these reasons, lasing is sensitive to the cell morphology and index variation, which enables identification of healthy from cancer cells based on their different spectral signatures.~~

Biological cells act in this novel experimental approach as the most significant amplification medium, and as a relevant part of the active medium. It follows that resulting lasing features – spectral and spatial modes– are closely related to the physico-chemical parameters of cells from which light amplification is originated, such as shape, size and local organization of organelles and biomaterials, hence the local refractive index distribution. We therefore expect the experimental conditions employed in this study to strengthen the structure-property relationship existing between cellular physico-chemical structure and cellular lasing.

3. Conclusion

In conclusion, we show that light amplification can be observed from dye-doped biological cells, without the need for traditional high-quality resonators or additional scatterers such as inorganic nanoparticles, and at an energy threshold of 500-1000 nJ/pulse. ~~Instead, biological cells to take an active role in the amplification of emission from embedded dyes, which we ascribe to the fluctuations of refractive index[15] taking place inside cells.~~ Numerical calculations demonstrate the role of refractive index contrast in cells in triggering light amplification, while a broader analogy with random lasing as observed from weakly scattering matrices[24] remains limited because of the low probability of multiple scattering.

Finally, by processing time series of spectra with principal component analysis (PCA), we extract spectral fingerprints ~~reveal that the same dye emits a random pattern of peaks that is characteristic for the specific cell type. Such, extracted with PCA,~~ that allow to separate spectral responses and to distinguish cancer from healthy Rattus glial cells with a very good degree of confidence.

The simplicity of the method used to achieve intense and highly efficient amplified emission, coupled to the rich information potential arising from the mixture of cellular refractive index contrast and dye concentration, pave the way for a rapid expansion of cell

triggered light amplification, which we envisage as a new analytical signal for biology and medicine.

4. Materials and methods

Sample preparation. All materials for cell culture were purchased from Gibco, otherwise notified. Rattus norvegicus brain glioma (C6 glioma) and rat primary cortical astrocyte cells (Astrocyte) were grown inside media containing 88% Dulbecco's Modified Eagle Medium, 10% Fetal Bovine Serum (FBS), 1% Penicillin-Streptomycin and 1% L-Glutamine 200 mM under 37oC and 5% of CO2 condition for 48 hours until reaching 90-95% cell confluency (concentration ca. $13x10^6$ cells/ml) of T-75 culture flask's surface (Corning). Subsequently, all cells were washed with Phosphate Buffer Solution, PBS twice followed by cell detachment by Trypsin-EDTA solution or StemPro® Accutase® cell dissociation reagent (Invitrogen). After cells were isolated from the surface, they were collected in Eppendorf tube and centrifuged (at 1,000 rpm) for 3 minutes. Supernatant was removed and cellular fixation was performed by immersing the cell pallet inside 1 ml 4% paraformaldehyde in PBS for 10 minutes. After the fixation, the cell solution was centrifuged for 3 minutes and the supernatant was removed subsequently. 500 μL rhodamine 6G staining solution (0.9 mM in DMSO (Sigma)) was added, mixed and the incubation time was done for 30 minutes. Cells were gently remixed

and approximately 10-20 μL of the cell-dye solution was moved to cell counting slides (Bio-Rad).

Fluorescence confocal microscopy. All of the fluorescence confocal images were acquired by means of a Zeiss LSM 710 confocal microscope system with 63x magnification, numerical aperture, NA 1.3 of Zeiss LCI Plan-NEOFLUAR water immersion objective lens (Zeiss GmbH). The samples were excited by continuous wave laser at 514 nm and the emission of the dye was collected in the range 520 nm to 735 nm.

Laser setup. A pulsed Nd:YAG laser (Spectra Physics, frequency of 10 Hz, pulse duration 8 ns) coupled to a Master Oscillator Power Amplifier (MOPA) system (Spectra Physics 200PRO) was employed and operated at 540 nm wavelength. The optical scheme (sketched in **Figure 1g**) includes the pump laser system followed by a sequence of optical attenuator filters, a Glan-Laser Polarizer (Thorlabs) to fine tune the pump intensity, a beam expander, a dichroic mirror (TRITC filter, reflection band 525 - 556 nm, transmission band 580 - 650 nm, Thorlabs), and an objective lens (10x, NA = 0.25, Thorlabs) to focus the beam and to collect light emitted from the sample, yielding a beam waist of about 20 μm at the focus position. A known fraction of the pump light is measured by means of a power meter to control the pump intensity. The light collected by the objective passes through the dichroic mirror and is partially reflected by a 50:50 beam splitter onto an Ocean Optics HR4000 Spectrometer with resolution 0.15 nm. Spectra are recorded in continuous mode with an acquisition time of 100

ms, and successively preprocessed and analyzed using Principal component analysis (PCA) statistics toolbox in Matlab. The light transmitted by the beam splitter passes through a tube lens and is imaged on a Charged Coupled Device (DCU224M CCD, Thorlabs).

Simulations. 3D-FDTD simulations of light scattering from a cell were performed using FDTD Solutions (Lumerical Inc.). Cells were modelled as spheres with a core-shell structure (12 μm in diameter), core of index 1.5 and a shell with index varying between 1.33 and 1.47. The core diameter was fixed to one third of the cell diameter in all simulations and symmetry boundary conditions were employed to significantly reduce the computation time. To calculate scattering cross-section, a total-field scattered-field (TFSF) light source was used to inject broadband light and a box of power monitors surrounding the cell were used to measure the scattered fields. Power monitors were also used to record the electric field intensity in the cross-section of the cell. The far-field distribution of the scattered fields was calculated using far-field projections from a closed box.

Supporting Information

Supporting Information is available from the Wiley Online Library or from the author.

Acknowledgements

The authors acknowledge the European Research Council Advanced grant award n. 2009-247365, the RU/TE-117/2412 and the Alexander von Humboldt Foundation for financial support.

Received: ((will be filled in by the editorial staff))
Revised: ((will be filled in by the editorial staff))
Published online: ((will be filled in by the editorial staff))

References

[1] T. Terai, T. Nagano, *Curr. Opin. Chem. Biol.* **2008**, *12*, 515.

[2] J. Zhang, R. E. Campbell, A. Y. Ting, R. Y. Tsien, *Nat. Rev. Mol. Cell Biol.* **2002**, *3*, 906.

[3] Y.-C. Chen, X. Fan, *Adv. Opt. Mater.* **2019**, *7*, 1900377.

[4] H. J. Oh, M. C. Gather, J.-J. Song, S. H. Yun, *Opt. Express* **2014**, *22*, 31411.

[5] S. Caixeiro, M. Gaio, B. Marelli, F. G. Omenetto, R. Sapienza, *Adv. Opt. Mater.* **2016**, *4*, 998.

[6] C. S. Wang, T. Y. Chang, T. Y. Lin, Y. F. Chen, *Sci. Rep.* **2014**, *4*, 1.

[7] D. Zhang, G. Kostovski, C. Karnutsch, A. Mitchell, *Org. Electron. physics, Mater. Appl.* **2012**, *13*, 2342.

[8] Q. Song, S. Xiao, Z. Xu, J. Liu, X. Sun, V. Drachev, V. M. Shalaev, O. Akkus, Y. L. Kim, *Opt. Lett.* **2010**, *35*, 1425.

[9] S. Nizamoglu, M. C. Gather, S. H. Yun, *Adv. Mater.* **2013**, *25*, 5943.

[10] Y. C. Chen, Q. Chen, T. Zhang, W. Wang, X. Fan, *Lab Chip* **2017**, *17*, 538.

[11] M. Humar, A. Dobravec, X. Zhao, S. H. Yun, *Optica* **2017**, *4*, 1080.

[12] M. C. Gather, S. H. Yun, *Nat. Photonics* **2011**, *5*, 406.

[13] M. Schubert, A. Steude, P. Liehm, N. M. Kronenberg, M. Karl, E. C. Campbell, S. J. Powis, M. C. Gather, *Nano Lett.* **2015**, *15*, 5647.

[14] M. Humar, S. H. Yun, *Nat. Photonics* **2015**, *9*, 572.

[15] M. Schubert, K. Volckaert, M. Karl, A. Morton, P. Liehm, G. B. Miles, S. J. Powis, M. C. Gather, *Sci. Rep.* **2017**, *7*, 1.

[16] A. Jonáš, M. Aas, Y. Karadag, S. Manioğlu, S. Anand, D. McGloin, H. Bayraktar, A. Kiraz, *Lab Chip* **2014**, *14*, 3093.

[17] Q. Chen, Y.-C. Chen, Z. Zhang, B. Wu, R. Coleman, X. Fan, *Lab Chip* **2017**, *17*, 2814.

[18] M. Humar, M. C. Gather, S.-H. Yun, *Opt. Express* **2015**, *23*, 27865.

[19] M. Karl, C. P. Dietrich, M. Schubert, I. D. W. Samuel, G. A. Turnbull, M. C. Gather, *J. Phys. D. Appl. Phys.* **2017**, *50*, DOI 10.1088/1361-6463/aa5367.

[20] Y.-C. Chen, X. Tan, Q. Sun, Q. Chen, W. Wang, X. Fan, *Nat. Biomed. Eng.* **2017**, *1*, 724.

[21] G. B. J. Dubelaar, J. W. M. Visser, M. Donze, *Cytometry* **1987**, *8*, 405.

[22] D. Watson, N. Hagen, J. Diver, P. Marchand, M. Chachisvilis, *Biophys. J.* **2004**, *87*, 1298.

[23] M. Kerker, H. Chew, P. J. McNulty, J. P. Kratohvil, D. D. Cooke, M. Sculley, M. P. Lee, *J. Histochem. Cytochem.* **1979**, *27*, 250.

[24] I. Z. Kozma, P. Krok, E. Riedle, *J. Opt. Soc. Am. B* **2005**, *22*, 1479.

[25] https://www.lumerical.com/products/fdtd-solutions

[26] V. Barna, L. De Cola, *Opt. Express* **2015**, *23*, 11936.

[27] D. S. Wiersma, *Nat. Phys.* **2008**, *4*, 359.

[28] Q. Zhang, L. Zhong, P. Tang, Y. Yuan, S. Liu, J. Tian, X. Lu, *Sci. Rep.* **2017**, *7*, 1.

[29] C. L. Curl, C. J. Bellair, T. Harris, B. E. Allman, P. J. Harris, A. G. Stewart, A. Roberts, K. A. Nugent, L. M. D. Delbridge, *Cytom. Part A* **2005**, *65*, 88.

[30] R. Barer, S. Joseph, *Q. J. Microsc. Sci.* **1954**, *95*, 399.

[31] J. S. Maier, S. A. Walker, S. Fantini, M. A. Franceschini, E. Gratton, *Opt. Lett.* **2008**, *19*, 2062.

[32] G. Mazarevica, T. Freivalds, A. Jurka, *J. Biomed. Opt.* **2002**, *7*, 244.

Supporting Movie MOVIE_S1

Click here to access/download
Supporting Information
MOVIE_S1.mov

Summary and TOC image

Figure 1

Click here to access/download

Production Data

Figure 1.tif

Figure 2

Figure 3

Click here to access/download

Production Data

Figure 3.tif

Figure 4

Figure 5